# Simple processing via thermal treatment and catalyst infiltration to enhance nickel electrode performance for liquid alkaline water electrolyzers

Guanzhi Wang, Grace Y. Lau, Xiong Peng, Michael C. Tucker*

Energy Conversion Group, Lawrence Berkeley National Laboratory, Berkeley, CA 94720

## Abstract

Two simple processes for enhancing liquid alkaline water electrolyzer performance are demonstrated. Both enhance 3D Ni electrodes by introducing a micron-scale rough structure throughout the bulk of the electrode. Oxidation/reduction relies on a simple thermal treatment cycle to create surface roughening through the volumetric expansion during NiO formation and volume contraction during reduction back to Ni metal. Catalyst infiltration introduces a washcoat of additional metal particles throughout the electrode, by flooding the electrode with catalyst precursor and converting it to micron-scale particles via a reducing thermal treatment. The largest improvement in performance (211 mV at 1.8 A $cm^{-2}$) is observed for infiltrated NiFe-3x catalyst. For Fe-free Ni-only electrodes, oxidation/reduction provides a larger improvement (157 mV at 1.8 A $cm^{-2}$) than infiltrated Ni-3X (106 mV at 1.8 A $cm^{-2}$). For both processes, the observed electrode surface structure and performance is quite sensitive to the thermal treatment temperature.

Keywords: LAWE; liquid alkaline electrolyzer; water electrolysis; nickel electrode

## Introduction

Liquid alkaline water electrolysis is a long-standing commercial technology for production of hydrogen from water feed and electrical power input. This technology is established at scale, and does not utilize expensive platinum-group metals as catalysts [1]. Ni is a preferred catalyst material, due to its low cost and chemical resistance to alkaline media [2]. Classic alkaline electrolyzers utilize a spacer between the porous diaphragm and the Ni-based electrodes, to reduce gas crossover especially at high operating pressure [3]. Recent interest in efficient generation of green hydrogen from renewable electricity has prompted a re-examination of the liquid alkaline water electrolyzer (LAWE) design. The goal is to develop a high-performance, durable next-generation LAWE design that is optimized for low-cost production of hydrogen from green electrons. An approach taken by the Hydrogen from Next-Generation Electrolyzers of Water (H2NEW) consortium is to utilize a zero- or near-zero gap design with the electrodes contacting the membrane to reduce ohmic losses, and to examine aspects of the electrode structure, catalyst composition, separator, operating protocols, and other aspects of the LAWE technology informed by modeling [4].

The Ni catalyst is typically structured as a macro-porous 3D material such as a perforated sheet, foam, mesh, or felt (or Ni coated on a steel substrate with these shapes) [2, 5]. It forms the electrochemically-active electrocatalyst region near the separator, and provides electrical connection between this region and the current collector or flowfield. Furthermore, in the case of zero-gap cell designs, the pores in the structure support transport of liquid to the active region, and removal of hydrogen or oxygen gas through the bulk of the electrode [5]. Therefore, the structure of the Ni electrode is critical for electrochemical performance of the LAWE device.

In particular, low electrochemical surface area (ECSA) of the Ni electrode limits performance. Many previous studies have employed various approaches and techniques to enhance the Ni ECSA. Raney Ni is a well-known high-surface area catalyst formed by dissolving Al or Zn from a Ni alloy, and has been widely applied to LAWEs [6-11]. Raney Ni catalyst powder was deposited as an ink directly on the separator diaphragm, resulting in a 270 mV cell potential improvement at 0.3 A $cm^{-2}$ [10]. Porous 3D Ni structures and planar electrodes have also been enhanced by various techniques. Ni foam was cleaned in three solutions, electroplated with NiZn, heat treated in hydrogen at 600 °C, and etched in HCl to obtain sub-micron pores that provided a 25-fold improvement in exchange current density [12]. Ni sheet was laser-structured to create sub-micron trenches and nano-scale protrusions that enhanced surface area by ~ 15 times and improved cell potential by 120 mV at 0.3 A $cm^{-2}$ [13]. DC/RF sputtering of Ni onto Ni foam created a 10 μm thick surface layer with nano-scale trenches, improving cell potential by ~200 mV at 0.8 A $cm^{-2}$ [9]. Ni mesh was hot-dip galvanized and leached in KOH, producing angular micron-scale roughness that remarkably improved cell potential by 470 mV at 0.5 A $cm^{-2}$ [14]. While these techniques to increase ECSA are generally effective at improving electrochemical activity, they are relatively complicated and resource-intensive to implement.

In this work, we demonstrate two simple techniques for increasing the performance of Ni foam electrodes. Both rely on enhancing the active surface area of the catalyst. The first, oxidation/reduction, utilizes thermal treatment in air to oxidize the Ni foam and impart micron-scale roughness on its surface. Reducing the NiO back to Ni retains the roughness while further introducing micron-scale pores. The second, catalyst infiltration, deposits additional Ni, Fe, or

NiFe mixture throughout the foam, which is then sintered and bonded to the foam through a reducing thermal treatment. Various process parameters are optimized, most notably the oxidation and sintering temperatures. The roughened electrodes are characterized with scanning electron microscopy (SEM) imaging, and tested as the anode in full cell LAWE devices. The anode is selected to demonstrate the improvement because anode kinetics are moderately more sluggish than cathode kinetics, and the anode is therefore more limiting for full cell performance [2, 15-17]. Both simple processes lead to significant improvement in LAWE performance.

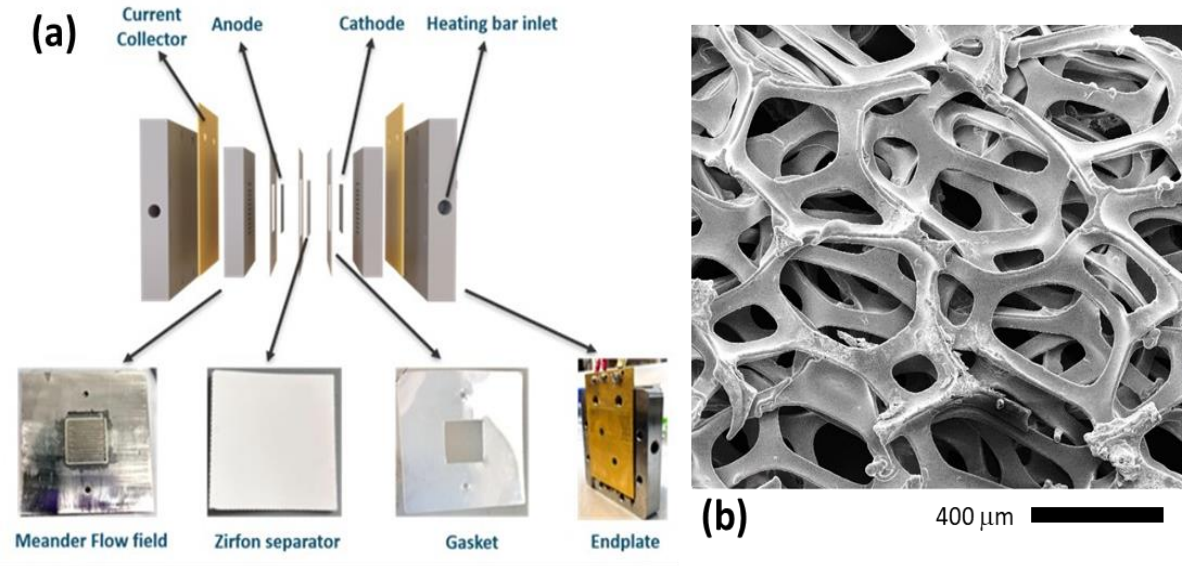


**Figure 1. LAWE and Ni electrode.** (a) Schematic of LAWE cell materials and testing hardware. (b) SEM image of as-received Ni foam.

## Experimental

Ni foam with 0.3 mm thickness, 110 pores per inch, and 97% porosity (MSE Supplies) was used as the baseline as-received electrode material throughout this work.

*Sample preparation – oxidation/reduction*

Controlled oxidation was carried out in ambient air in a box furnace (Vulcan 3-550). Ni foam samples were placed horizontally on an alumina plate in the hot zone of the furnace at 400 to 1000 °C and held for 2 h. The ramping rate for heating and cooling was 10 °C $min^{-1}$. The extent of oxidation from Ni to NiO was determined by weighing the samples. It was found that the extent of oxidation was much more sensitive to oxidation temperature than to hold time, so temperature was selected as the variable for optimization. After oxidation, the samples were reduced to Ni in a tube furnace with metal flange caps and alumina tube (MTI GSL-1100X), and a mineral oil bubbler to prevent backflow of air into the tube. The sample temperature (calibrated at the sample location) was held at 600 °C for 2h, with 5 °C $min^{-1}$ heating and cooling rates. The tube was flushed with 100 sccm flowrate of 2% $H_2$/98% Ar using a mass flow controller (Alicat). After reduction, complete conversion back to Ni metal was confirmed by weighing the samples and comparing to the starting weight.

*Sample preparation – infiltrated catalyst coating*

Catalysts were coated throughout the bulk of the Ni foam using a standard infiltration technique commonly applied to solid oxide fuel cells [18, 19]. Ni, Fe, or NiFe (50/50 mole ratio) were deposited into the Ni foam from an aqueous nitrate salt solution. Triton-X-100 (Sigma Aldrich) surfactant was dissolved in deionized water (1.2:10 wt) by stirring overnight with a magnetic stir bar. This solution was then mixed with nitrate salts (Sigma Aldrich) and glycine chelating agent (Sigma Aldrich) on a shaker table until the salts were completely dissolved. Typical mixing ratios were (Ni) 4.4 g Ni nitrate hexahydrate, 0.26 g glycine, with 1 g solution, (Fe) 3.9 g Fe nitrate

nonahydrate, 0.17 g glycine, with 1 g solution, or (NiFe) 1.4 g Ni nitrate hexahydrate and 1.9 g Fe nitrate nonahydrate, 0.17 g glycine, with 1 g solution. Ni foam was then soaked in these catalyst precursor solutions, excess solution was drained off, and the samples were transferred into the box furnace described above. The samples were held at 90 °C for 1h to dry the solution, and then fired at 400 °C for 1 h with 10 °C $min^{-1}$ heating and cooling rate to convert the nitrate salts to metal oxides. This process was completed 3 or 10 times to adjust the total catalyst loading, represented in the text as for example "Ni-3x". The metal oxides were then reduced to metals using the same reducing tube furnace setup described above, with 2 h hold at various temperatures from 500 to 900 °C. Lower reducing temperatures were not tested, as we found that the catalyst particles are not bonded well at lower temperatures.

*Electrochemical testing*

A standard Fuel Cell Technology cell with two 5 $cm^2$ Ni serpentine flow fields for both anode and cathode were used for LAWE single cell construction. Ni electrodes mentioned above were used on the cathode and anode sides accordingly. A commercial Zirfon (AGFA Perl UTP 500) was used as the separator membrane. When assembling, ETFE gaskets (CS Hyde) with different thickness were added around the electrodes and separator used to seal the cell. Hot 7M KOH (80 ℃, diluted from 85% from Fisher Chemical) at 20 ml/min was fed to both anode and cathode when the cell was heated to 80 ℃.

All the electrochemical testing was performed with a Biologic VSP potentiostat. Polarization curves were collected through chronopotentiometric technique with each constant current held for 20 s, and the average potential over the last 5 s of each current was used for the steady-state potential. Galvanostatic electrochemical impedance spectroscopy (GEIS) was conducted at each

current to determine the ohmic resistance and charge transfer characteristic. The testing was done at a frequency range of 1 Hz to 100 kHz with the signal amplitude of 5% of the applied current. The high frequency resistance (HFR) was determined through GEIS fitting with an equivalent circuit including a series combination of a resistor and two RCPEs. The electrochemical active specific area (ECSA) estimation was conducted in a three-electrode system in 1M KOH solution, with the Ni electrodes as working electrode, graphite rod as reference electrode and Ag/AgCl reference electrode. The ECSA of electrodes were qualitatively estimated by the electrochemical double layer capacitance ($C_{dl}$) estimation from the cyclic voltammogram (CV) curves in the non-Faradic region at various scan rates. The $C_{dl}$ was calculated according to equation (1):

$$C_{dl}=i / v \quad (1)$$

where $i$ is the double layer current densities collected from CV curves at the same potential, and $v$ is the corresponding scan rate.

*Characterization*

As-received and processed samples were imaged using scanning electron microscopy (SEM) and energy-dispersive x-ray mapping (EDX). A JEOL 7500F SEM was used for imaging. Weight gain was determined using a high-precision analytical balance with 0.01 mg accuracy (Ohaus Pioneer).

## Results and Discussion

*1. Oxidation/reduction of Ni foam*

Ni foam was oxidized and then reduced to create a roughened surface, Figs. 2 and S1. This treatment does not impact the macroscopic structure of the foam, but does affect the Ni surface throughout the depth of the foam. The extent of oxidation was controlled by the oxidation temperature in air, Fig 2a, and is consistent with previous studies of Ni oxidation kinetics [20]. At 400 °C, minimal oxidation occurs. As the temperature increases to 700 °C, the oxidation weight gain slowly increases to about 5%. The oxidation increases dramatically from 700 to 800 °C, then increases more slowly up to 1000 °C. Full oxidation of Ni to NiO results in a theoretical 27% weight gain, which was achieved at 1000 °C. The rapid increase in weight gain from 700 to 800 °C is accompanied by a transition from partial to complete oxidation of the Ni surface. At 700 °C and below, partial roughening of the surface is observed (Figs. 2c and S1), with the grain boundaries showing preferential roughening. At 800 °C and above, the entire surface is roughened (Figs. 2d and S1). A distinctly roughened and pitted surface is observed, with feature size around 0.5 to 1 μm. In contrast, the as-received Ni foam surface is characterized by grains of 2 to 10 μm size, and is relatively smooth (Fig. 2b). The surface becomes rough as it oxidizes (Fig. S2), due to NiO crystallization and the volume expansion associated with the Ni to NiO transition. When the NiO is reduced back to Ni metal, the volume reduction introduces pores and pits in the surface and the roughness is retained. This reduction step and the higher oxidation temperatures introduce additional surface area compared to the 600 °C oxidation-only process reported previously [21]. Based on these observations, foams oxidized at 600, 700, and 900 °C were chosen to represent minimally oxidized, partially oxidized, and completely oxidized Ni surface, respectively.

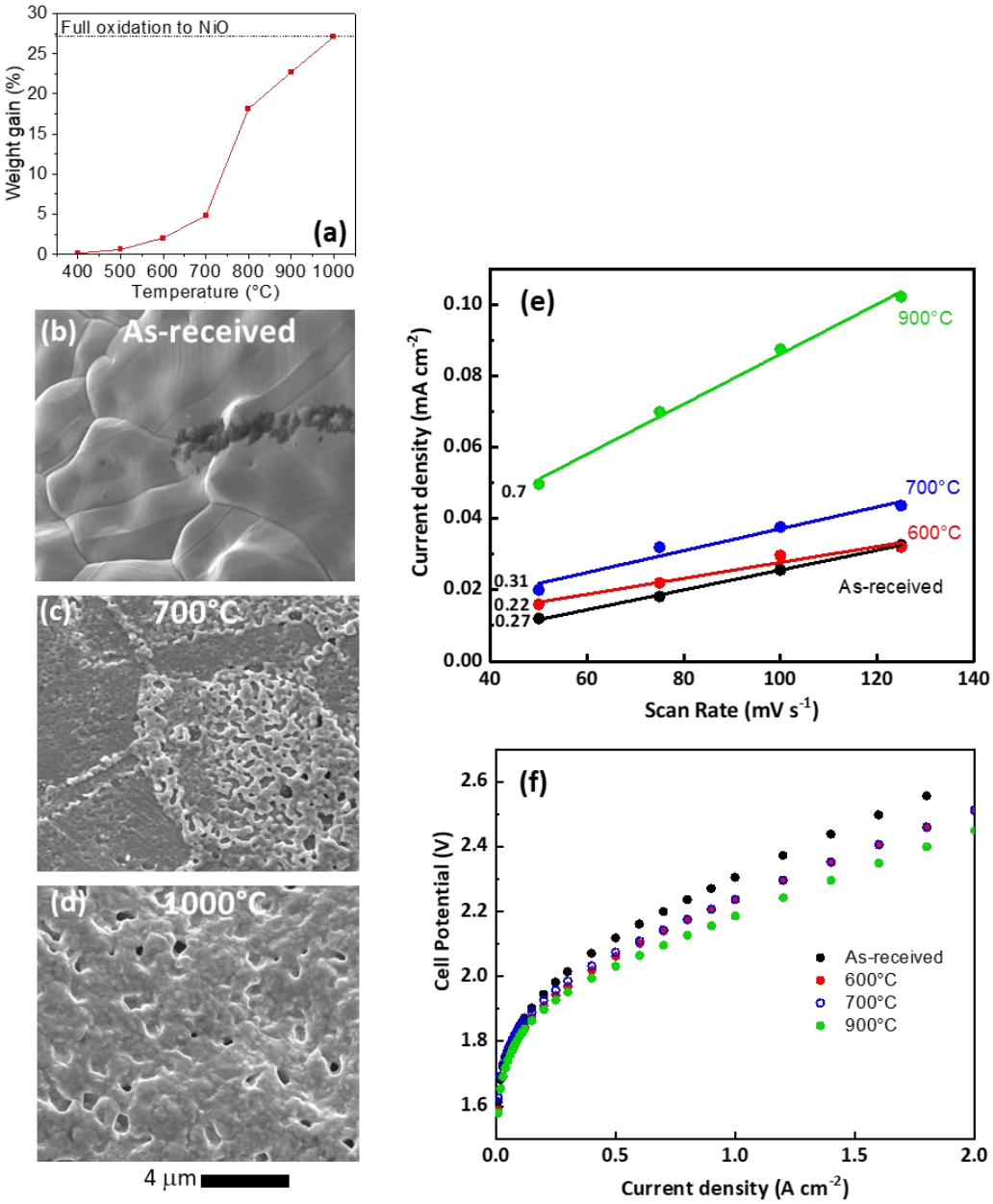


**Figure 2. Oxidation/reduction processing of Ni foam.** (a) Weight gain of Ni foam after oxidizing in air for 2 h at various temperatures. The 27% weight gain expected for complete oxidation of Ni to NiO is indicated as a dashed line. SEM images of Ni foam (b) as-received and after oxidation at (c) 700 °C or (d) 1000 °C followed by reduction at 600 °C. Comparison of as-received and roughened Ni foams using (e) 3-electrode cell CV results (see Fig S2 for full data set) with double-layer capacitance (mF $cm^{-2}$) indicated in black text, and (f) Full LAWE cell polarization curves at 80 °C.

The enhanced surface roughness observed after oxidation/reduction processing yields higher electrochemical activity, Fig 2e,f. Qualitatively speaking, the double layer capacitance at the electrode/electrolyte interfaces could represent the electrode ECSA for OER. A 3-electrode setup was used to characterize the double layer capacitance, Fig. 2e, similar to the technique reported previously for Ni roughened by sputtering and laser ablation [9, 13]. The slope increases dramatically from the 0.27 mF $cm^{-2}$ observed for baseline as-received Ni foam to 0.7 mF $cm^{-2}$ for the foam oxidized at 900 °C. The full cell LAWE performance is significantly improved by the enhanced anode surface area, Fig 2f. The as-received Ni foam achieves 2.56 V at 1.8 A $cm^{-2}$. The foams with partial roughening (600 and 700 °C) improve cell potential by 95 mV at 1.8 A $cm^{-2}$. The foam with full roughening (900 °C) yields a 157 mV improvement, the largest improvement observed for any of the pure Ni samples tested in this study. This improvement is within the range observed for other electrode roughening techniques (see Introduction section).

*2. Ni foam coated with catalyst via infiltration*

Micron-scale Ni, Fe, and NiFe catalyst particles were deposited throughout the bulk of Ni foams using an infiltration technique. Aqueous nitrate salt precursors were flooded into the Ni foam, dried, fired in air, and then reduced to metal particles at various temperatures in the range 500 to 900 °C. Lower temperature was not considered, as minimal bonding between the particles and Ni foam would likely compromise mechanical integrity of the catalyst coatings. For the case of Ni catalyst, particles coat the entire foam surface, Figs. 3 and S4. After 3 cycles of infiltration followed by reduction, the Ni catalyst loading is approximately 5wt% based on the original foam weight. A nearly continuous layer of Ni particles is observed, and increasing the infiltration cycles to 10 does not visibly increase the surface roughness or coverage (Fig S5). Similar particulate

coatings are observed for Fe and NiFe catalysts, Fig S5. After firing at 500 °C, the Ni particles are approximately 1 μm particle size, and appear to be well-bonded to each other and to the Ni foam, Fig. 3a. After firing at 700 °C, the catalyst particles are noticeably coarsened, reducing the total surface area, Fig 3b. Upon firing at higher temperatures, the surface particles are mostly (800 °C, Fig S4) or completely (900 °C, Fig 3c) consumed into the foam structure due to sintering diffusion, leaving a smooth surface that looks similar to the as-received foam. Sintering is driven by surface energy, so the Ni particles are incorporated into the main body of the foam through densification and grain growth, similar to standard densification of a Ni powder pellet.

The full cell LAWE performance is significantly improved by the added catalyst coatings, Fig 4. For Ni-3x, the best performance is achieved for the 600 °C reducing temperature, Fig 4a. At lower temperature, the minimal extent of sintering may limit electronic connectivity and mechanical integrity of the deposited catalyst. As temperature increases above 600 °C, over-sintering reduces the catalyst area (as observed with SEM above), and the performance decreases. At 900 °C, where no catalyst particles remain and the surface is smooth (Fig. 3c), the performance is almost identical to the as-received Ni foam (2.56 V at 1.8 A $cm^{-2}$). A similar trend with increasing temperature is observed for NiFe-3x, Fig. 4b.

Consistent with the SEM observations above, adding more Ni by increasing the number of infiltration cycles does not further improve performance, Fig. 4c. Presumably, once the Ni foam surface is completely covered with additional Ni particles (Ni-3x), adding more Ni particles (Ni-10x) does not further increase the electrochemically active surface area. This may be because only the outermost layer of catalyst particles participates in the reaction, or because subsequent infiltration cycles fill in the pores, and densify the catalyst coating. Based on these results, Ni-3x

reduced at 600 °C was chosen as the optimum processing conditions for infiltrated Ni catalyst. The full cell voltage at 1.8 A $cm^{-2}$ was improved by 106 mV. This is slightly less beneficial than the oxidation/reduction processing discussed above in Section 1.

Adding Fe to the catalyst coating (NiFe-3x), or replacing Ni with Fe (Fe-3x) further improves performance, Fig 4d. NiFe-3x provides the best performance of all the samples studied here, achieving 211 mV improvement at 1.8 A $cm^{-2}$. This is consistent with previous reports that Fe enhances catalytic activity in LAWE, however there is uncertainty about Fe stability during long-term operation [22-26]. The presence of Fe also enables SEM/EDX analysis to show that the catalyst is well distributed throughout the foam (Fig. S6).

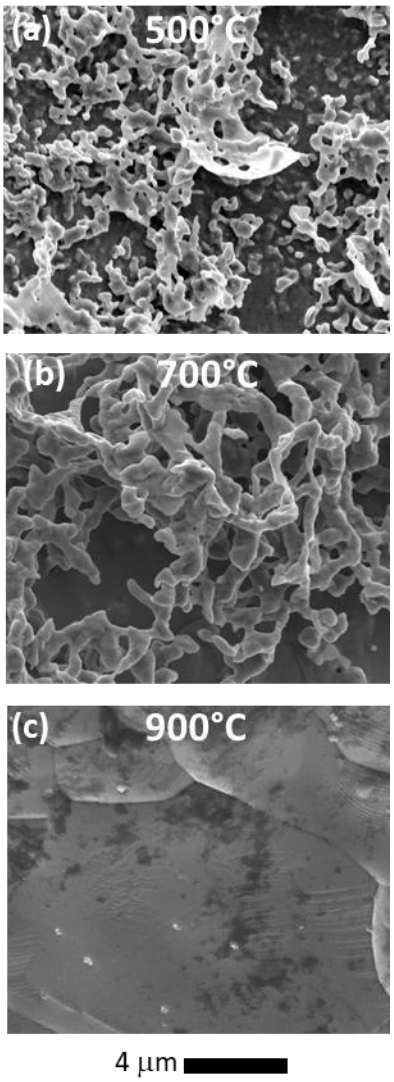


**Figure 3. Catalyst-coated Ni foams.** SEM images of Ni foam coated with Ni-3x via infiltration, and then reduced to Ni metal at (a) 500 °C, (b) 700 °C, or (c) 900 °C.

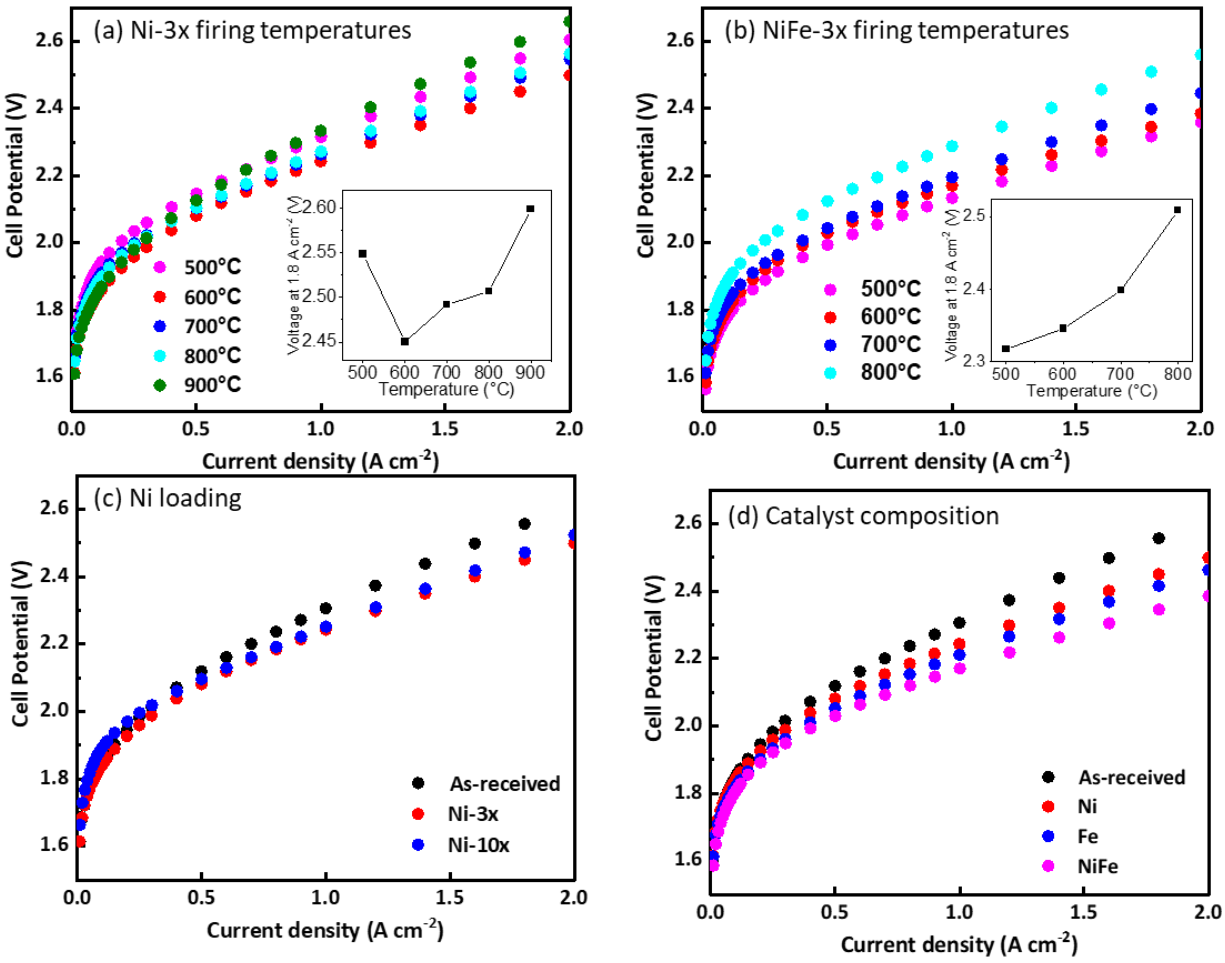


**Figure 4. Performance of catalyst-coated Ni foams.** Comparison of as-received and catalyst-coated Ni foams using full LAWE cell polarization curves at 80 °C. Impact of (a) reducing firing temperature for Ni-3x, (b) reducing firing temperature for NiFe-3x, (c) Ni catalyst loading (all fired at 600 °C), and (d) catalyst composition (all 3x, and fired at 600 °C). Insets to (a,b) show the voltage at 1.8 A $cm^{-2}$ for each firing temperature.

## Conclusions

Two simple processes for enhancing LAWE performance were demonstrated. Both enhanced 3D Ni foam electrodes by introducing micron-scale rough structure throughout the bulk of the electrode. Oxidation/reduction relies on a simple thermal treatment cycle to create surface roughening through the volumetric expansion during NiO formation and contraction during reduction back to Ni metal. Catalyst infiltration introduces a washcoat of additional metal particles throughout the electrode, by flooding the electrode with catalyst precursor and converting it to micron-scale particles via a reducing thermal treatment. The largest improvement in performance (211 mV at 1.8 A $cm^{-2}$) was observed for infiltrated NiFe-3x catalyst. For Fe-free Ni-only electrodes, oxidation/reduction provided a larger improvement (157 mV at 1.8 A $cm^{-2}$) than infiltrated Ni-3X (106 mV at 1.8 A $cm^{-2}$). This is a welcome result, as the oxidation/reduction process does not require any additional material and is considered to be a simpler and more easily scalable process than catalyst infiltration. For both processes, the observed electrode surface structure and performance is quite sensitive to the thermal treatment temperature. This suggests further optimization of the thermal treatment parameters (time, temperature, atmosphere, etc.) may be fruitful. This work establishes the utility of the oxidation/reduction and catalyst infiltration processes for enhancing LAWE Ni foam anode performance. Future work will include a comprehensive study extending these techniques to the cathode and other Ni electrode structures (felt, sintered particles, etc.), and assessing the long-term durability.

**Acknowledgements**

The authors thank Eric Lees for helpful discussion. This material is based upon work supported by the U.S. Department of Energy's Office of Energy Efficiency and Renewable Energy (EERE) under the H2 from the Next-generation Electrolyzers of Water (H2NEW) consortium for funding under Contract Number DE-AC02-05CH11231. This document was prepared as an account of work sponsored by the United States Government. While this document is believed to contain correct information, neither the United States Government nor any agency thereof, nor the Regents of the University of California, nor any of their employees, makes any warranty, express or implied, or assumes any legal responsibility for the accuracy, completeness, or usefulness of any information, apparatus, product, or process disclosed, or represents that its use would not infringe privately owned rights. Reference herein to any specific commercial product, process, or service by its trade name, trademark, manufacturer, or otherwise, does not necessarily constitute or imply its endorsement, recommendation, or favoring by the United States Government or any agency thereof, or the Regents of the University of California. The views and opinions of authors expressed herein do not necessarily state or reflect those of the United States Government or any agency thereof or the Regents of the University of California. This manuscript has been authored by an author at Lawrence Berkeley National Laboratory under Contract No. DE-AC02-05CH11231 with the U.S. Department of Energy. The U.S. Government retains, and the publisher, by accepting the article for publication, acknowledges, that the U.S. Government retains a non-exclusive, paid-up, irrevocable, world-wide license to publish or reproduce the published form of this manuscript, or allow others to do so, for U.S. Government purposes.

## References


[1] Buttler A, Spliethoff H. Current status of water electrolysis for energy storage, grid balancing and sector coupling via power-to-gas and power-to-liquids: A review. Renewable and Sustainable Energy Reviews. 2018;82:2440-54.
[2] Zeng K, Zhang D. Recent progress in alkaline water electrolysis for hydrogen production and applications. Progress in Energy and Combustion Science. 2010;36:307-26.
[3] Trinke P, Haug P, Brauns J, Bensmann B, Hanke-Rauschenbach R, Turek T. Hydrogen Crossover in PEM and Alkaline Water Electrolysis: Mechanisms, Direct Comparison and Mitigation Strategies. Journal of The Electrochemical Society. 2018;165:F502.
[4] Shviro M, Pivovar B, Badgett A, Smith C, Serov A, Peng X, et al. H2NEW: Hydrogen (H2) from Next-generation Electrolyzers of Water LTE Task 9: Liquid alkaline. DOE HFTO Annual Merit Review and Peer Evaluation Meeting. Arlington, VA2023.
[5] Phillips R, Dunnill Charles W. Zero gap alkaline electrolysis cell design for renewable energy storage as hydrogen gas. RSC Advances. 2016;6:100643-51.
[6] Chade D, Berlouis L, Infield D, Cruden A, Nielsen PT, Mathiesen T. Evaluation of Raney nickel electrodes prepared by atmospheric plasma spraying for alkaline water electrolysers. International Journal of Hydrogen Energy. 2013;38:14380-90.
[7] Colli AN, Girault HH, Battistel A. Non-Precious Electrodes for Practical Alkaline Water Electrolysis. Materials 2019; 12:1336.
[8] Gannon WJF, Dunnill CW. Raney Nickel 2.0: Development of a high-performance bifunctional electrocatalyst. Electrochimica Acta. 2019;322:134687.
[9] Han W-B, Kim I-S, Kim M, Cho WC, Kim S-K, Joo JH, et al. Directly sputtered nickel electrodes for alkaline water electrolysis. Electrochimica Acta. 2021;386:138458.
[10] Karacan C, Lohmann-Richters FP, Shviro M, Keeley GP, Müller M, Carmo M, et al. Fabrication of High Performing and Durable Nickel-Based Catalyst Coated Diaphragms for Alkaline Water Electrolyzers. Journal of The Electrochemical Society. 2022;169:054502.
[11] Martínez WM, Fernández AM, Cano U, Sandoval J A. Synthesis of nickel-based skeletal catalyst for an alkaline electrolyzer. International Journal of Hydrogen Energy. 2010;35:8457-62.
[12] Zhang J, Zhou Y, Zhang S, Li S, Hu Q, Wang L, et al. Electrochemical Preparation and Post-treatment of Composite Porous Foam NiZn Alloy Electrodes with High Activity for Hydrogen Evolution. Scientific Reports. 2018;8:15071.
[13] Poimenidis IA, Tsanakas MD, Papakosta N, Klini A, Farsari M, Moustaizis SD, et al. Enhanced hydrogen production through alkaline electrolysis using laser-nanostructured nickel electrodes. International Journal of Hydrogen Energy. 2021;46:37162-73.
[14] Schalenbach M, Kasian O, Mayrhofer KJJ. An alkaline water electrolyzer with nickel electrodes enables efficient high current density operation. International Journal of Hydrogen Energy. 2018;43:11932-8.
[15] Haverkort JW, Rajaei H. Voltage losses in zero-gap alkaline water electrolysis. Journal of Power Sources. 2021;497:229864.
[16] Kibria MF, Mridha MS. Electrochemical studies of the nickel electrode for the oxygen evolution reaction. International Journal of Hydrogen Energy. 1996;21:179-82.
[17] Kibria MF, Mridha MS, Khan AH. Electrochemical studies of a nickel electrode for the hydrogen evolution reaction. International Journal of Hydrogen Energy. 1995;20:435-40.

[18] Connor PA, Yue X, Savaniu CD, Price R, Triantafyllou G, Cassidy M, et al. Tailoring SOFC Electrode Microstructures for Improved Performance. Advanced Energy Materials. 2018;8:1800120.
[19] Dogdibegovic E, Cheng Y, Shen F, Wang R, Hu B, Tucker MC. Scaleup and manufacturability of symmetric-structured metal-supported solid oxide fuel cells. Journal of Power Sources. 2021;489:229439.
[20] Atkinson A, Taylor RI, Hughes AE. A quantitative demonstration of the grain boundary diffusion mechanism for the oxidation of metals. Philosophical Magazine A. 1982;45:823-33.
[21] Karacan C, Lohmann-Richters FP, Keeley GP, Scheepers F, Shviro M, Müller M, et al. Challenges and important considerations when benchmarking single-cell alkaline electrolyzers. International Journal of Hydrogen Energy. 2022;47:4294-303.
[22] Demnitz M, Lamas YM, Garcia Barros RL, de Leeuw den Bouter A, van der Schaaf J, Theodorus de Groot M. Effect of iron addition to the electrolyte on alkaline water electrolysis performance. iScience. 2024;27.
[23] Wang J, Gao Y, Kong H, Kim J, Choi S, Ciucci F, et al. Non-precious-metal catalysts for alkaline water electrolysis: operando characterizations, theoretical calculations, and recent advances. Chemical Society Reviews. 2020;49:9154-96.
[24] Zhou D, Li P, Xu W, Jawaid S, Mohammed-Ibrahim J, Liu W, et al. Recent Advances in Non-Precious Metal-Based Electrodes for Alkaline Water Electrolysis. ChemNanoMat. 2020;6:336-55.
[25] He Z, Zhang J, Gong Z, Lei H, Zhou D, Zhang N, et al. Activating lattice oxygen in NiFe-based (oxy)hydroxide for water electrolysis. Nature Communications. 2022;13:2191.
[26] Ou Y, Twight LP, Samanta B, Liu L, Biswas S, Fehrs JL, et al. Cooperative Fe sites on transition metal (oxy)hydroxides drive high oxygen evolution activity in base. Nature Communications. 2023;14:7688.